Liver Fat Content and T2*: Simultaneous Measurement by Using Breath-hold Multiecho MR Imaging at 3.0 T—Feasibility[1]

Declan P. O'Regan, MRCP, FRCR
Martina F. Callaghan, PhD
Marzena Wylezinska-Arridge, PhD
Julie Fitzpatrick, DCR(R)
Rossi P. Naoumova, MD, PhD
Joseph V. Hajnal, PhD
Stephan A. Schmitz, MD, PhD

Research ethics committee approval was obtained for this study, and written informed consent was obtained from all participants. The purpose was to prospectively evaluate the feasibility of breath-hold multiecho in- and out-of-phase magnetic resonance (MR) imaging for simultaneous lipid quantification and T2* measurement. A spoiled gradient-echo sequence with seven echo times alternately in phase and out of phase was used at 3.0 T. Imaging was performed in a lipid phantom, in five healthy volunteers (all men; mean age, 37 years), and in five obese individuals with hyperlipidemia or diabetes (four men, one woman; mean age, 53 years). A biexponential curve-fitting model was used to derive the relative signal contributions from fat and water, and these results were compared with results of liver proton MR spectroscopy, the reference standard. There was a significant correlation between multiecho and spectroscopic measurements of hepatic lipid concentration ($r^2 = 0.99$, $P < .001$). In vivo, the T2* of water was consistently longer than that of fat and reliably enabled the signal components to be correctly assigned. In the lipid phantom, the multiecho method could be used to determine the fat-to-water ratio and the T2* values of fat and water throughout the entire range of fat concentrations. Multiecho imaging shows promise as a method of simultaneous fat and T2* quantification.

[1] From the Imaging Sciences Department and Clinical Research Facility, MRC Clinical Sciences Centre, Faculty of Medicine, Imperial College, Hammersmith Hospital Campus, Du Cane Road, London W12 0NN, United Kingdom. Received May 18, 2007; revision requested July 19; revision received August 3; accepted September 7; final version accepted September 28. Supported by grants from Bayer Schering Pharma and Philips Medical Systems. **Address correspondence to** D.P.O. (e-mail: *declan.oregan@imperial.ac.uk*).

Accurate noninvasive assessment of liver fat content is an important tool in the evaluation of patients with hepatic steatosis (1). Lipid quantification with magnetic resonance (MR) imaging relies on the difference in resonant frequency between fat and water molecules. With gradient-echo sequences, the signal intensity is at a maximum when the transverse magnetization vectors of fat and water within the voxel are in phase and at a minimum when the vectors are out of phase (2). Single- and dual-echo techniques have previously been used to estimate lipid content within the liver (2–9) and adrenal glands (10). However, signal intensity loss on in-phase images caused by the presence of liver iron is a potential pitfall in the determination of liver fat percentage by using dual-echo imaging (11). A separate sequence is therefore required to correct for global T2* effects. A further limitation is that dual-echo methods do not enable differentiation of whether the dominant component is fat or water, so an additional sequence with either gradient-echo imaging or breath-hold spectroscopy is required to resolve this (12,13).

In contrast, multiecho imaging has the potential to enable more accurate and efficient measurement of tissue fat content in a single sequence. The signal intensity variation in a multiecho acquisition would be expected to depend on the individual T2* decays of the fat and water components, as well as a periodic oscillation of signal intensity between in-phase and out-of-phase echo times dependent on the fat-to-water ratio (14–17). A rapid single sequence allowing accurate tissue fat quantification as well as T2* measurement would be of potential value in lipid deposition disorders.

Thus, the aim of our study was to prospectively evaluate the feasibility of breath-hold multiecho in- and out-of-phase MR imaging for simultaneous lipid quantification and T2* measurement.

Advances in Knowledge

- Unlike with dual-echo methods, with multiecho MR imaging, fat measurement can be performed without the need to acquire a separate T2* map, and the signal components may be correctly assigned to fat and water on the basis of their different T2* values.
- Results of fat quantification in the liver by using a multiecho technique correlate highly ($r^2 = 0.99$, $P < .001$) with those of T2-corrected proton MR spectroscopy.

Materials and Methods

Financial support was given by Bayer Schering Pharma (Newbury, Berkshire, England) and Philips Medical Systems (Best, the Netherlands). The authors had control of the data and information submitted for publication.

Lipid Phantom Study

A phantom was constructed by pouring equal volumes of mineral oil (liquid petrolatum; Johnson and Johnson, New Brunswick, NJ) and water into a cylindric container (6). The water was doped with 10 mmol/L copper sulfate solution to shorten its T2. An oblique imaging plane was chosen that passed through the boundary of the two immiscible layers. Therefore, the oil-to-water ratio within a voxel at a given point in the image varied along a continuous gradient from pure oil to pure water (Fig 1). The oil percentage at a given point was determined through cross-reference to a coronal high-spatial-resolution T1-weighted gradient-echo MR image obtained perpendicular to the plane of the fluid layers. The sequence parameters were as follows: flip angle, 80°; field of view, 320 mm; section thickness, 4 mm; receiver bandwidth, 1930 Hz/pixel; acquired voxel size, 0.5 × 0.5 × 4 mm; repetition time msec/echo time msec, 16/2.3; number of signal averages, two; and a frequency-encoding direction oriented parallel to the oil and water interface.

Implication for Patient Care

- Multiecho MR imaging shows promise as a method for simultaneous fat and T2* quantification in the liver.

Human Participants

The study was undertaken with the approval of the Hammersmith Hospital research ethics committee, and written informed consent was obtained from all study participants. Five obese individuals with a history of hyperlipidemia or diabetes (four men, one woman; mean age, 53 years; range, 35–67 years; mean body mass index, 36.2 kg/m^2; range, 33–40 kg/m^2) were enrolled. The control group consisted of five healthy volunteers with no history of excess alcohol use (<30 g per day) or diabetes (five men; mean age, 37 years; range, 32–44 years; mean body mass index, 25.0 kg/m^2; range, 22–30 kg/m^2).

Multiecho Sequence

The MR imaging studies were performed with a 3.0-T MR imaging system (Intera; Philips) operating with Release 1.7 software. A software patch was installed to enable multiecho imaging. The same scaling factors were applied to each image in the multiecho acquisition. The maximum gradient strength was 31 mT/m, and the maximum slew rate was 200 mT/m/msec. Imaging was performed by using a breath-hold spoiled gradient-echo sequence with a seven-echo readout, resulting in a total acqui-

Published online before print
10.1148/radiol.2472070880

Radiology 2008; 247:550–557

Abbreviation:
ROI = region of interest

Author contributions:
Guarantor of integrity of entire study, D.P.O.; study concepts/study design or data acquisition or data analysis/interpretation, all authors; manuscript drafting or manuscript revision for important intellectual content, all authors; manuscript final version approval, all authors; literature research, D.P.O.; clinical studies, D.P.O., J.F., R.P.N., J.V.H., S.A.S.; experimental studies, D.P.O., M.F.C., M.W., J.F., J.V.H., S.A.S.; statistical analysis, D.P.O., M.F.C., M.W.; and manuscript editing, D.P.O., M.F.C., M.W., R.P.N., S.A.S.

See Materials and Methods for pertinent disclosures.

sition time of 4 seconds for a single section. The multiecho sequence parameters were as follows: flip angle, 20°; field of view, 320 mm; section thickness, 10 mm; receiver bandwidth, 780 Hz/pixel; acquired voxel size, 2.5 × 2.5 × 10 mm; repetition time, 17 msec; and number of signal averages, two. Proton spectroscopy studies have revealed that the chemical shift of intrahepatic lipid relative to water is 3.4 ppm (18); hence, in vivo, the first echo time (TE) chosen was 1.15 msec, with a ΔTE of 1.15 msec (TEs: 1.15, 2.30, 3.45, 4.60, 5.75, 6.90, and 8.05 msec). The chemical shift in the oil phantom was determined as 3.5 ppm, and the ΔTE was reduced to 1.12 msec (TEs: 1.12, 2.24, 3.36, 4.48, 5.60, 6.72, and 7.84 msec) for these experiments.

Body imaging was performed by one technologist (J.F., with 10 years of experience in MR imaging). A six-channel phased-array receiver coil was used, and images were acquired in held expiration. A single-section multiecho sequence was performed in a transverse plane passing through the liver and spleen, superior to the main portal vein. Higher-order shimming was used, with a volume manually placed over the liver. Participant tolerance of the examination, signs of peripheral nerve stimulation, and image quality were monitored.

Liver spectroscopy was performed by one operator (M.W., with 10 years of experience in spectroscopy). Spectroscopy was performed during the same study as multiecho imaging. Single-voxel spectroscopic measurement of intrahepatic fat levels was performed according to a protocol previously validated at 1.5 T (19). An 8-cm^3 cubic volume of interest was placed over the right lobe of the liver, avoiding intrahepatic blood vessels. The Q-body coil was used to transmit and receive. A point-resolved spectroscopy sequence (20) without water suppression was used for spatial localization and spectra acquisition. To correct for T2 decay, three consecutive spectra were acquired with echo times of 40, 60, and 135 msec. The repetition time was 2000 msec, and 32 signals were acquired.

Data Analysis: Modeling of Fat and Water Phase Interference

In tissues containing lipid and water, there will be oscillation in signal intensity as a function of echo time. The signal intensity of each component will also show T2* decay. The magnitude signal intensity (|S|) may therefore be modeled with the following equation:

$$|S| = |S_w e^{-t/T2^*_w} + S_f e^{-t/T2^*_f + i\Delta\omega t}|$$

where S_w and S_f are the components of the signal from water and fat, respectively, and $T2^*_w$ and $T2^*_f$ are their respective decay constants, while t is the time after excitation and $\Delta\omega$ is the difference in frequency between fat and water. To reduce the number of degrees of freedom in the model, the frequency difference between fat and water was considered to be 3.4 ppm. The signal components from water (S_w) and fat (S_f), as well as their respective T2* decay constants ($T2^*_w$ and $T2^*_f$), were modeled with an iterative curve-fitting technique by using the Levenberg-Marquardt algorithm (21) and software (SigmaPlot, version 10; SPSS, Chicago, Ill). For the purpose of comparison with results of MR spectroscopy, the lipid content was expressed as a percentage of the total signal as follows: lipid content percentage = $100\% \cdot [S_f/(S_w + S_f)]$.

A comparison was made with fat estimation performed by using a conventional dual-echo method by analyzing only the first pair of in-phase and out-of-phase echoes with the following equation: lipid content percentage = $[(S_{IP} - S_{OP}) \cdot 100\%]/$

Figure 1

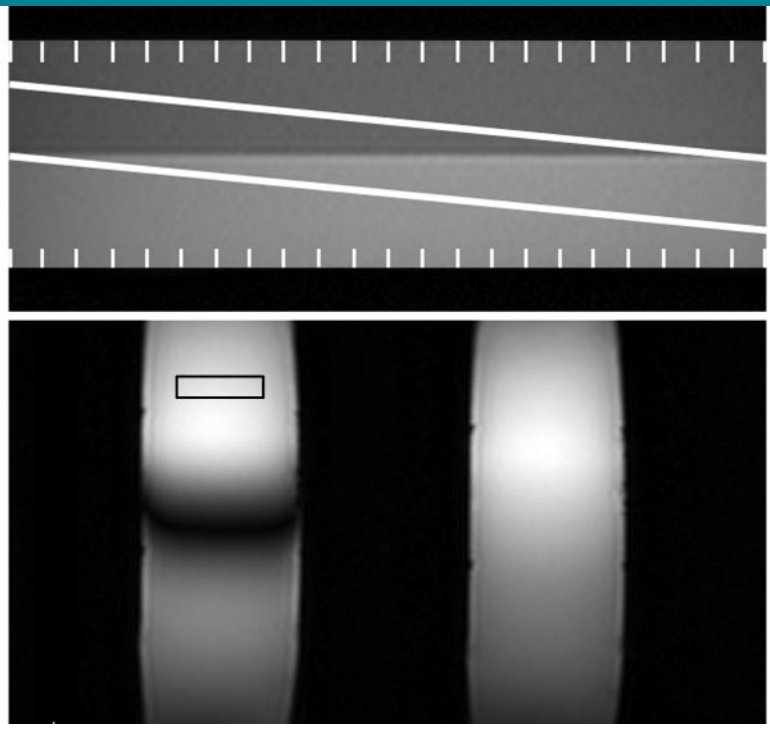

Figure 1: Oil and water phantom: immiscible layers of mineral oil and water were used to simulate a range of oil-to-water ratios. Top: An oblique MR imaging section (16/2.3; flip angle, 80°; frequency encoding direction, left to right) was positioned across the interface of the two layers, and 11 points along this gradient from 0% to 100% oil were used to position the regions of interest (ROIs) on the multiecho images. Bottom left: Out-of-phase image (17/1.15; flip angle, 20°) shows position of first rectangular ROI and demonstrates signal cancellation in voxels containing fat and water. Bottom right: In-phase image (17/2.3; flip angle, 20°) is shown for comparison.

$(2 \cdot S_{IP})$, where S_{IP} and S_{OP} are the signal intensities on the in-phase and out-of-phase images, respectively (6).

Image Analysis

The raw image data were exported from the imaging unit for off-line reconstruction and were converted to "Analyze" format by using software (Matlab, version 7.0; Mathworks, Natick, Mass). Analysis of multiecho imaging studies was performed by one operator (D.P.O., with 6 years of experience in MR imaging) with a Pentium 4 3.0-GHz computer by using software (ImageJ; National Institutes of Health, Bethesda, Md). The coronal T1-weighted image of the oil and water phantom was used to identify the relative proportions of fat and water along the oblique imaging section. Eleven equally spaced divisions along this gradient, from 0% to 100% oil, were cross-referenced to a position on the multiecho images. Each ROI placed on the multiecho images measured 40 × 10 pixels. On the liver images, a circular ROI (30 mm in diameter) was placed in the same location as the spectroscopy voxel, avoiding vascular structures. In each case, the mean signal intensity was measured at each echo time. The curve-fitting algorithm using the biexponential model was used to derive the fat fraction, as well as the component T2* decays for fat and water. An automated pixel-by-pixel analysis was performed to obtain color-coded parametric maps of liver fat and water percentages, also by using the Matlab software.

Figure 2

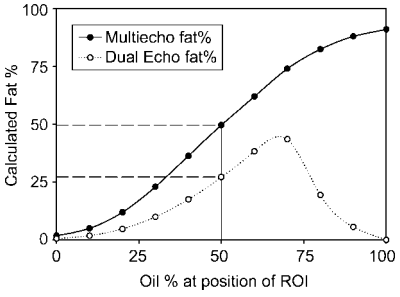

Figure 2: Graph shows results of fat percentage estimation across range of oil-to-water ratios in the oil and water phantom by using the dual-echo and multiecho sequences. The component with the longer T2* has been assigned to water in the multiecho analysis. The dual-echo plot assumes that water is the dominant component. Dotted lines = calculated fat percentage at 50:50 oil-to-water ratio for each method.

Reference Standard Liver Spectroscopy

The phase-corrected spectra were analyzed in the time domain by using the AMARES algorithm included in the MRUI software package (22). Resonance fitting was performed by M.W. to obtain signal intensities for lipid (S_f) and water (S_w). Exponential regression analysis of the peak amplitudes at each echo time was used for T2 decay correction. Lipid fraction was derived from S_f and S_w in the same manner as that used with the multiecho technique.

Statistical Analysis

Statistical analysis was performed by using software (SPSS, version 12, SPSS; and MedCalc, version 9, MedCalc Software, Mariakerke, Belgium). Results are presented as mean values ± 1 standard deviation. Bland-Altman plots (23) were used to analyze the agreement between multiecho and MR spectroscopic estimations of liver fat content and be-

Figure 3

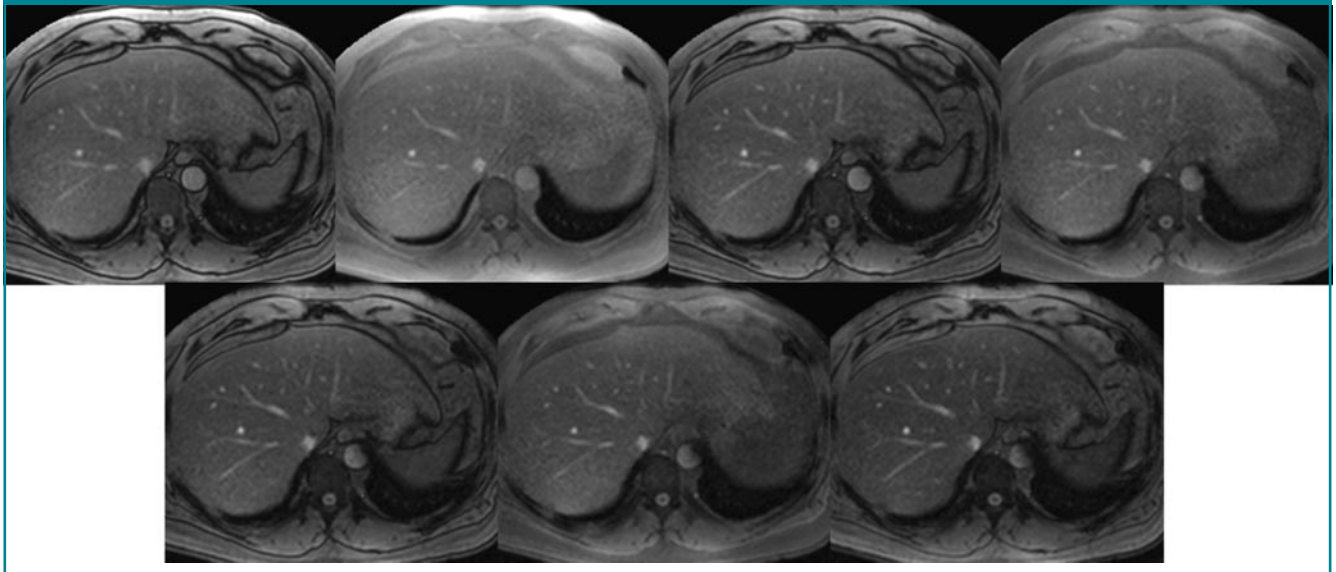

Figure 3: Transverse breath-hold multiecho MR imaging acquisition (17/1.15–8.05; flip angle, 20°; field of view, 320 mm; section thickness, 10 mm) in liver with seven readouts. Images are alternately out of phase and in phase from left to right in each row. Image quality is maintained throughout the range of echo times.

tween multiecho and dual-echo estimations of liver fat content. The correlation between liver fat concentration as determined with multiecho imaging and concentration as determined with MR spectroscopy was assessed by using linear least-squares regression. The means of the in vivo $T2^*_w$ and $T2^*_f$ values were compared by using a paired-samples t test. $P < .05$ was considered to indicate a significant difference.

Results

Oil and Water Phantom

The multiecho sequence modeling derived the two signal intensity components and their respective T2* values throughout the range of oil-to-water ratios. The two signal intensity components (oil and water) had mean T2* values of 94.4 msec ± 11.6 and 5.1 msec ± 2.3, respectively. The correct interpretation of the oil-to-water ratio at each position along the phantom was obtained if the component with the longer T2* value was assumed to be water. The dual-echo method does not allow a determination of the dominant component, and, accordingly, less signal cancellation was seen at each end of the oil concentration gradient. At the midpoint of the phantom, with a 50:50 oil-to-water ratio, the multiecho method derived a fat content of 49%; the dual-echo method derived a fat content of 27% (Fig 2).

In Vivo Multiecho Sequence and MR Spectroscopy

MR imaging was well tolerated by all participants; there was good image quality throughout the range of echo times (Fig 3). Specific absorption rates were within specified limits (4.0 W/kg), and no peripheral nerve stimulation was reported. The proton spectra demonstrated satisfactory line widths, with water and lipid peaks at 4.7 and 1.3 ppm, respectively.

The multiecho sequence modeling converged on a fit for S_w and S_f and the individual $T2^*_w$ and $T2^*_f$ components in all subjects but one (Table). This healthy volunteer had a fat content of only 1.3% at multiecho imaging, and the $T2^*_f$ could not be derived. In the patient group, the mean hepatic fat fraction determined with multiecho imaging was 17.7% ± 7.3, while the mean water T2* value was 16.0 msec ± 4.1 and the mean lipid T2* value was 7.4 msec ± 2.1. In the volunteer group, the mean hepatic fat fraction was 2.7% ± 1.4, while the mean water T2* value was 21.8 msec ± 11.7 and the mean lipid T2* value was 4.6 msec ± 1.8. Among all subjects, there was a significant difference between the mean $T2^*_w$ and $T2^*_f$ values ($P < .05$), and the $T2^*_w$ value was consistently greater than the $T2^*_f$ value (Figs 4, 5).

Bland-Altman analysis revealed a systematic underestimation of fat content with the dual-echo method compared with the multiecho method, with the mean limits of agreement being −2.6% ± 2.4 (1.96 times the standard deviation) (Fig 6). Results of least-squares analysis indicated a significant correlation between multiecho and spectroscopic measurements of hepatic lipid ($y = 0.94x + 0.63$, $r^2 = 0.99$, $P < .001$) (Fig 7). A Bland-Altman analysis revealed that the mean limits of agreement of fat quantification with the multiecho method compared with quantification with MR spectroscopy was 0.03% ± 1.5 (1.96 times the standard deviation) (Fig 8).

A computer simulation was used to measure the expected error in fat estimation with the dual-echo method in a system with biexponential decay. Representative values for the T2* of fat and water obtained in this group of subjects were used in the simulation (Fig 9). For instance, this demonstrated that at 30% fat, the dual-echo method would be expected to produce a 6% (uncorrected for T2*) or 4% (with global T2* correction) underestimation of true fat content.

Results of MR Spectroscopy, Dual-Echo Modeling, and Multiecho Modeling of Liver Fat Content in Healthy Volunteers and Obese Individuals

Group and Participant No.	Fat Percentage at MR Spectroscopy	Fat Percentage with Dual-Echo Modeling	Fat Percentage with Multiecho Modeling	$T2^*_w$ with Multiecho Modeling (msec)	$T2^*_f$ with Multiecho Modeling (msec)
Healthy volunteers					
1	1.1	<0	1.3	11.8	—
2	1.6	<0	2.0	16.0	6.0
3	2.6	<0	3.1	19.2	6.1
4	1.3	<0	2.0	41.8	2.6
5	3.7	0.5	4.8	20.0	3.6
Obese individuals					
6	11.0	7.2	10.7	20.0	7.0
7	10.6	7.0	10.2	17.7	5.0
8	20.3	16.5	20.5	11.2	6.5
9	20.7	19.3	19.7	19.0	10.6
10	28.7	25.1	27.5	12.1	8.0

Note.—In participants 1–4, the first out-of-phase image had higher signal intensity than the in-phase image for the dual-echo analysis.

Figure 4

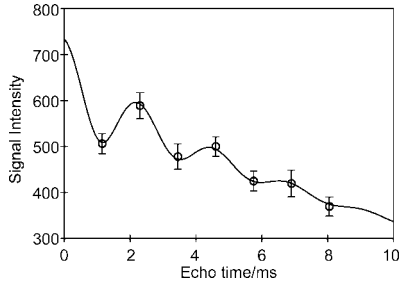

Figure 4: Plot of mean signal intensity in ROI in steatotic liver with the multiecho sequence shows the biexponential model's convergence on a best-fit curve.

Discussion

Our results demonstrate the feasibility of using in-phase and out-of-phase multiecho imaging to quantify liver fat content and T2* with one sequence. Coregistered pixel maps of liver fat content and T2* values may be automatically generated. The technique shows excellent agreement with T2-corrected single-voxel spectroscopy, and each set of images is obtained in a short breath hold. Multiexponential analysis of fat-water systems has been shown to be feasible with spin-echo sequences in phantoms (15), and gradient-echo sequences have been used to assess bone marrow composition at 1.5 T (16) and lower field strengths (17). However, to our knowledge, there are no published reports of the use of multiecho phase interference techniques to quantify liver fat content.

Dual-echo imaging is in routine clinical use for the semiquantitative assessment of liver fat content. However, multiecho sequences overcome a number of limitations of conventional dual-echo techniques for fat quantification. First, the method allows a determination of the fat-to-water ratio that is corrected for T2* effects without the need for additional mapping sequences and potential image misregistration. This may be a substantial limitation of dual-echo imaging in patients with cirrhosis because of the T2*-shortening effects of iron deposition (11). Dual-echo quantification also fails at low fat fractions when T2* effects predominate over fat-water signal cancellation. The multiecho technique also allows a further correction to be made for the differential T2* decays of fat and water, although the effect on fat estimation is expected to be only approximately 5% in vivo. However, the ability to distinguish between the water and fat signal components overcomes an important limitation of dual-echo fat estimation. The dual-echo approach requires an additional gradient-echo sequence with different T1 weighting (12) or visual inspection of results of breath-hold spectroscopy (13) to confirm whether fat or water is the majority component. Despite these steps, there remains ambiguity between 45% and 55% fat content (6), and spectroscopic results that are uncorrected for T2 decay may have similar limitations. Our findings indicate that in the liver, the T2* of water is consistently longer than that of fat at 3.0 T, and this allows the signals to be correctly assigned if the liver fat content is at least 2%. Below this level, noise within the image prevents the signal contribution of fat from being modeled.

In this study, the multiecho sequence was optimized for the quantification of tissue fat. However, as the sequence

Figure 5

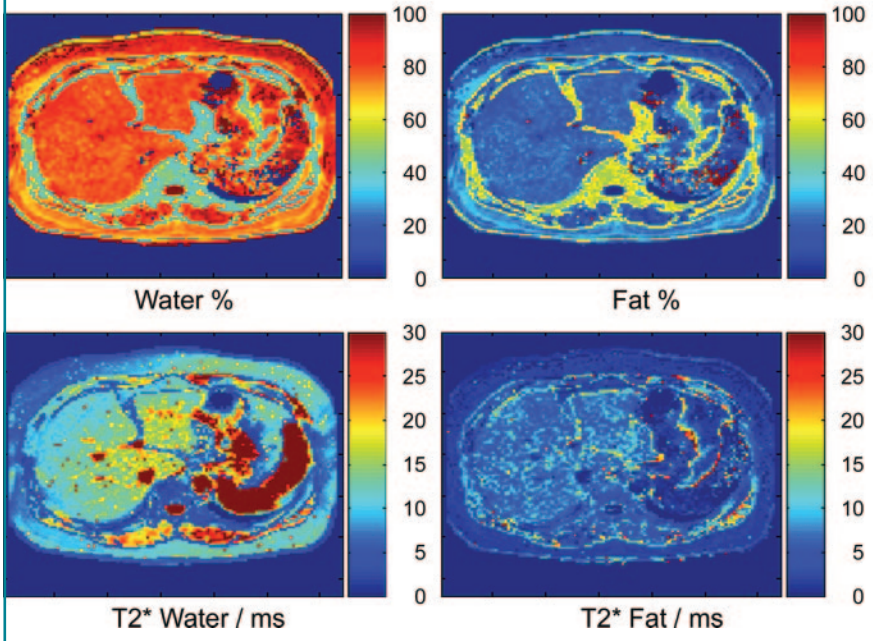

Figure 5: Color-coded parametric maps of multiecho data in patient with hepatic steatosis. Coregistered images of water and fat percentage, as well as their respective T2* values (in milliseconds), were derived from a single multiecho acquisition. Color bars and numbers in top row = percentages; those in bottom row = milliseconds.

Figure 6

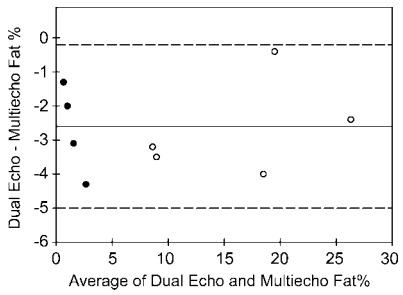

Figure 6: Bland-Altman plot of agreement of liver fat assessment in vivo between dual-echo and multiecho MR imaging. The mean of each pair of measurements is plotted against their difference. Dashed lines = 95% confidence intervals, solid line = mean value, ● = healthy volunteers, ○ = obese individuals.

Figure 7

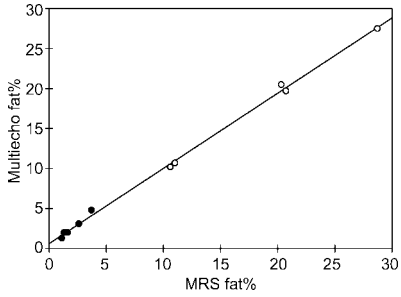

Figure 7: Graph shows relationship between fat estimation in the liver performed by using multiecho MR imaging technique and that performed by using MR spectroscopy *(MRS)* ($y = 0.94x + 0.63$, $r^2 = 0.99$, $P < .001$). ● = Healthy volunteers, ○ = obese individuals.

Figure 8

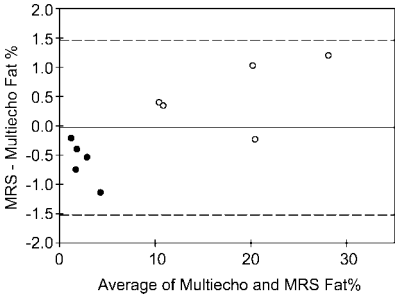

Figure 8: Bland-Altman plot of agreement of liver fat assessment in vivo between MR spectroscopy and multiecho imaging. The mean of each pair of measurements is plotted against their difference. Dashed lines = 95% confidence intervals, solid line = mean value, ● = healthy volunteers, ○ = obese individuals.

Figure 9

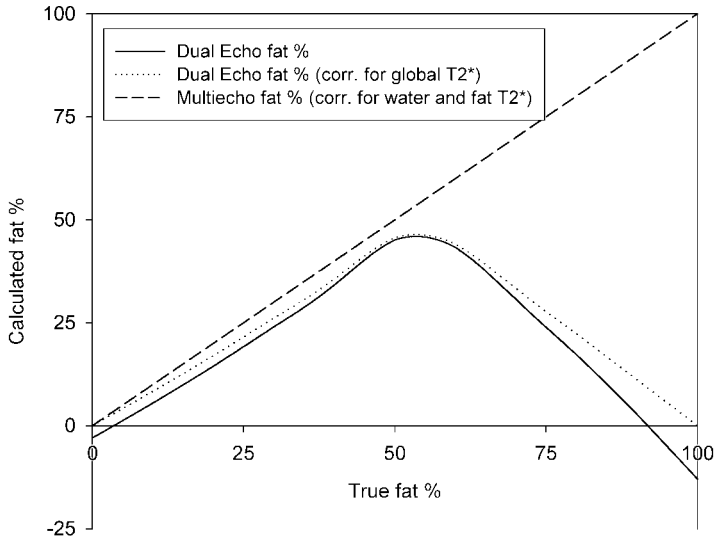

Figure 9: Graph shows simulation of expected differences in fat percentage calculation by using three methods. The biexponential model was used to simulate in- and out-of-phase signal intensities throughout the entire range of fat-to-water ratios. Physiologic T2* values ($T2^*_w$, 20 msec; $T2^*_f$, 5 msec) estimated from in vivo data have been used in the model. For this comparison, T1 effects were not included in the model. The ideal correlation was assumed to be given by the multiecho method, which corrects for the individual T2* decays of fat and water. The first in-phase and out-of-phase echo times from the simulation were used for fat quantification with the dual-echo method, with water assumed to be the dominant component. These values were then corrected *(corr.)* for global T2* decay by using regression analysis of the in-phase echo times.

also inherently measures tissue T2*, it has the potential to provide coregistered information on hepatic iron content. Gradient multiecho techniques, with an arbitrary echo time interval, have been histologically validated in the assessment of hepatic iron overload at 1.5 T (24) and enable a reliable assessment of global tissue T2* (25–27). However, the echo times chosen must allow adequate sampling of the T2* decay curve, and this will depend on the severity of the iron overloading being investigated. Multiecho imaging with biexponential analysis has the advantage over simple relaxometry of being able to model the effects of both T2* decay and fat-water phase interference on signal intensity.

Our study had limitations. MR spectroscopy was chosen as a reference standard for the multiecho technique because it has been validated at 1.5 T (18,28–30). Early experience in liver MR spectroscopy at 3.0 T demonstrated it to be a promising technique (31,32), and it has the potential to achieve improved signal-to-noise characteristics and greater spectral resolution. However, these advantages may be offset by increased line widths due to increased field inhomogeneities and decreased T2 relaxation times (33). No histologic correlation of hepatic steatosis was made in our study because the patients in the study group did not have an indication for liver biopsy. Furthermore, the measurement of lipid in histologic samples relies on semiquantitative methods (34,35). The ratio calculated with the multiecho sequence reflects the molar concentrations of resonating hydrogen nuclei in fat and water, but this may be readily converted into fat content by liver weight or volume for comparison with biopsy data (19).

The biexponential model was not extended to include T1 decay constants for fat and water. To reduce the T1 weighting of the sequence while maintaining an adequate signal-to-noise ratio, a shallow flip angle of 20° was chosen. The tissue T1 relaxation time of the liver is also significantly longer at 3.0 T than at 1.5 T (36), and this may also reduce the effects of T1 contrast on fat quantification. The chemical shift was also chosen as a fixed parameter in the model and was used to determine the optimum echo times for maximum and minimum phase cancellation. A potential underestimation of lipid concentration would be obtained if the actual chemical shift differed from this value. The model also assumed that there was a single lipid resonance and did not allow for the effects of separate methyl and methlylene groups, for instance. The accuracy of the curve-fitting algorithm will also depend on the metric used to measure goodness of fit, as well as the effects of noise in the data.

The oil phantom demonstrated the behavior of the multiecho sequence over a wide range of oil concentrations. Chemical shift will displace the fat and water voxels, but these errors were minimized by the choice of frequency encoding direction and by not including the edges of the phantom in our ROI measurements. The radiofrequency excitation pulse is a sinc function, and the shape of the section profile may modulate the transition from oil to water voxels. Flip angle inhomogeneity and susceptibility effects at the boundary of the layers may also affect the linearity between the calculated and the measured oil concentration. The difference in T2* of the oil and wa-

ter components was also greater than that seen in vivo.

In conclusion, results of our feasibility study show that multiecho MR imaging provides a technique for quantifying liver fat content that is highly correlated with T2-corrected proton spectroscopy. In contrast to dual-echo methods, multiecho imaging overcomes the potential errors due to T2* effects and enables the correct assignment of the fat and water signal components in a sequence performed during a single breath hold. This technique also allows the simultaneous acquisition of coregistered fat and T2* maps of the liver.

References

1. Clark JM, Brancati FL, Diehl AM. Nonalcoholic fatty liver disease. Gastroenterology 2002;122:1649–1657.
2. Fishbein MH, Gardner KG, Potter CJ, Schmalbrock P, Smith MA. Introduction of fast MR imaging in the assessment of hepatic steatosis. Magn Reson Imaging 1997;15:287–293.
3. Javor ED, Ghany MG, Cochran EK, et al. Leptin reverses nonalcoholic steatohepatitis in patients with severe lipodystrophy. Hepatology 2005;41:753–760.
4. Kawamitsu H, Kaji Y, Ohara T, Sugimura K. Feasibility of quantitative intrahepatic lipid imaging applied to the magnetic resonance dual gradient echo sequence. Magn Reson Med Sci 2003;2:
47–50.
5. Rinella ME, McCarthy R, Thakrar K, et al. Dual-echo, chemical shift gradient-echo magnetic resonance imaging to quantify hepatic steatosis: implications for living liver donation. Liver Transpl 2003;9:851–856.
6. Hussain HK, Chenevert TL, Londy FJ, et al. Hepatic fat fraction: MR imaging for quantitative measurement and display—early experience. Radiology 2005;237:1048–1055.
7. Pilleul F, Chave G, Dumortier J, Scoazec JY, Valette PJ. Fatty infiltration of the liver: detection and grading using dual T1 gradient echo sequences on clinical MR system. Gastroenterol Clin Biol 2005;29:1143–1147.
8. Chan DC, Watts GF, Ng TW, Hua J, Song S, Barrett PH. Measurement of liver fat by magnetic resonance imaging: relationships with body fat distribution, insulin sensitivity and plasma lipids in healthy men. Diabetes Obes Metab 2006;8:698–702.
9. Qayyum A, Goh JS, Kakar S, Yeh BM, Merriman RB, Coakley FV. Accuracy of liver fat quantification at MR imaging: comparison of out-of-phase gradient-echo and fat-saturated fast spin-echo techniques—initial experience. Radiology 2005;237:507–511.
10. Namimoto T, Yamashita Y, Mitsuzaki K, et al. Adrenal masses: quantification of fat content with double-echo chemical shift in-phase and opposed-phase FLASH MR images for differentiation of adrenal adenomas. Radiology 2001;218:642–646.
11. Westphalen AC, Qayyum A, Yeh BM, et al. Liver fat: effect of hepatic iron deposition on evaluation with opposed-phase MR imaging. Radiology 2007;242:450–455.
12. Hollingsworth KG, Abubacker MZ, Joubert I, Allison ME, Lomas DJ. Low-carbohydrate diet induced reduction of hepatic lipid content observed with a rapid non-invasive MRI technique. Br J Radiol 2006;79:712–715.
13. Chang JS, Taouli B, Salibi N, Hecht EM, Chin DG, Lee VS. Opposed-phase MRI for fat quantification in fat-water phantoms with 1H MR spectroscopy to resolve ambiguity of fat or water dominance. AJR Am J Roentgenol 2006; 187:W103–W106.
14. Haacke EM. Magnetic resonance imaging: physical principles and sequence design. New York, NY: Wiley-Liss, 1999.
15. Kamman RL, Bakker CJ, van Dijk P, Stomp GP, Heiner AP, Berendsen HJ. Multi-exponential relaxation analysis with MR imaging and NMR spectroscopy using fat-water systems. Magn Reson Imaging 1987;5:381–392.
16. Wehrli FW, Ford JC, Attie M, Kressel HY, Kaplan FS. Trabecular structure: preliminary application of MR interferometry. Radiology 1991;179:615–621.
17. Derby K, Kramer DM, Kaufman L. A technique for assessment of bone marrow composition using magnetic resonance phase interference at low field. Magn Reson Med 1993;29: 465–469.
18. Szczepaniak LS, Babcock EE, Schick F, et al. Measurement of intracellular triglyceride stores by H spectroscopy: validation in vivo. Am J Physiol 1999;276(5 pt 1):E977–E989.
19. Szczepaniak LS, Nurenberg P, Leonard D, et al. Magnetic resonance spectroscopy to measure hepatic triglyceride content: prevalence of hepatic steatosis in the general population. Am J Physiol Endocrinol Metab 2005; 288:E462–E468.
20. Bottomley PA. Spatial localization in NMR spectroscopy in vivo. Ann N Y Acad Sci 1987; 508:333–348.
21. Marquardt DW. An algorithm for least squares estimation of parameters. J Soc Ind Appl Math 1963;11:431–441.
22. Vanhamme L, van den Boogaart A, Van Huffel S. Improved method for accurate and efficient quantification of MRS data with use of prior knowledge. J Magn Reson 1997;129:35–43.
23. Bland JM, Altman DG. Statistical methods for assessing agreement between two methods of clinical measurement. Lancet 1986;1:307–310.
24. Anderson LJ, Holden S, Davis B, et al. Cardiovascular T2-star (T2*) magnetic resonance for the early diagnosis of myocardial iron overload. Eur Heart J 2001;22:2171–2179.
25. Bonkovsky HL, Rubin RB, Cable EE, Davidoff A, Rijcken TH, Stark DD. Hepatic iron concentration: noninvasive estimation by means of MR imaging techniques. Radiology 1999;212:227–234.
26. Westwood MA, Anderson LJ, Firmin DN, et al. Interscanner reproducibility of cardiovascular magnetic resonance T2* measurements of tissue iron in thalassemia. J Magn Reson Imaging 2003;18:616–620.
27. Wood JC, Enriquez C, Ghugre N, et al. MRI R2 and R2* mapping accurately estimates hepatic iron concentration in transfusion-dependent thalassemia and sickle cell disease patients. Blood 2005;106:1460–1465.
28. Longo R, Pollesello P, Ricci C, et al. Proton MR spectroscopy in quantitative in vivo determination of fat content in human liver steatosis. J Magn Reson Imaging 1995;5:281–285.
29. Thomsen C, Becker U, Winkler K, Christoffersen P, Jensen M, Henriksen O. Quantification of liver fat using magnetic resonance spectroscopy. Magn Reson Imaging 1994;12:487–495.
30. Longo R, Ricci C, Masutti F, et al. Fatty infiltration of the liver: quantification by 1H localized magnetic resonance spectroscopy and comparison with computed tomography. Invest Radiol 1993;28:297–302.
31. Ishii M, Yoshioka Y, Ishida W, et al. Liver fat content measured by magnetic resonance spectroscopy at 3.0 tesla independently correlates with plasminogen activator inhibitor-1 and body mass index in type 2 diabetic subjects. Tohoku J Exp Med 2005;206:23–30.
32. Fischbach F, Thormann M, Ricke J. (1)H magnetic resonance spectroscopy (MRS) of the liver and hepatic malignant tumors at 3.0 Tesla [in German]. Radiologe 2004;44:1192–1196.
33. Barker PB, Hearshen DO, Boska MD. Single-voxel proton MRS of the human brain at 1.5T and 3.0T. Magn Reson Med 2001;45:765–769.
34. Sanyal AJ. AGA technical review on nonalcoholic fatty liver disease. Gastroenterology 2002;123:1705–1725.
35. Franzen LE, Ekstedt M, Kechagias S, Bodin L. Semiquantitative evaluation overestimates the degree of steatosis in liver biopsies: a comparison to stereological point counting. Mod Pathol 2005;18:912–916.
36. de Bazelaire CM, Duhamel GD, Rofsky NM, Alsop DC. MR imaging relaxation times of abdominal and pelvic tissues measured in vivo at 3.0 T: preliminary results. Radiology 2004; 230:652–659.